

# Low-complexity Rounded KLT Approximation for Image Compression

A. P. Radünz \*

F. M. Bayer †

R. J. Cintra ‡

Tue 30<sup>th</sup> Nov, 2021 @ 2:29am

## Abstract

The Karhunen-Loève transform (KLT) is often used for data decorrelation and dimensionality reduction. Because its computation depends on the matrix of covariances of the input signal, the use of the KLT in real-time applications is severely constrained by the difficulty in developing fast algorithms to implement it. In this context, this paper proposes a new class of low-complexity transforms that are obtained through the application of the round function to the elements of the KLT matrix. The proposed transforms are evaluated considering figures of merit that measure the coding power and distance of the proposed approximations to the exact KLT and are also explored in image compression experiments. Fast algorithms are introduced for the proposed approximate transforms. It was shown that the proposed transforms perform well in image compression and require a low implementation cost.

## Keywords

Approximate KLT, Image compression, Karhunen-Loève transform, Low-complexity transforms

## 1 Introduction

We are living in the era where colossal amounts of data are generated every day, the Big Data era [1]. With increasing computational demands for analyzing large masses of data in real-time, the development of low-complexity signal processing methods became an area of great interest [2]. In this context, data compression techniques are the main tools for reducing data dimensionality, a necessary requisite for efficient data transmission and storage. There are several methods for data compression [3, 4] and they are all based on the same principle of reducing or removing redundancy from the input data [5]. In particular, transform-based compression methods generally map the input data into smaller output data [6].

Among several transforms found in the literature, the Karhunen-Loève transform (KLT) [7–9] has the distinction of being capable of completely decorrelate the input signal in the transform domain [9, 10]. In fact, the KLT is the optimal linear transform that minimizes the mean squared error in data compression for maximum energy concentration in a few coefficients of the output signal. Although mathematically optimal, the KLT has limited applicability, because its derivation depends on the covariance matrix of the input data, thus precluding or hindering the development of fast algorithms for its computation. However, if the input data is a first-order Markov process with known correlation coefficient  $\rho$ , then the associate covariance matrix is deterministically known and fast algorithms are possible [11]. Nonetheless, even when a fast algorithm is possible, it requires multiplications by a significant amount of irrational numbers, increasing the computational cost of the algorithm. To the best of our knowledge, literature is scarce in methods devoted to the efficient implementation of the KLT [12–14]. Our approach differs from the literature mainly because we consider first-order Markov signals for different values of  $\rho$ . In this way, depending on the correlation coefficient of the input signal, we will have a low-complexity transform.

The KLT is mathematically linked to the DCT [9, 15]. In fact,

the DCT is itself an asymptotic approximation for the KLT when (i) the input data is first-order Markovian and (ii) the correlation coefficient of the input signal tends the unity [15]. In contrast to the KLT, the definition of DCT does not depend on the input signal, which allows the development of fast algorithms computationally efficient. Thus, DCT became widely adopted in image and video compression standards such as JPEG [16], MPEG [17], and HEVC [18], for example. However, even considering state-of-the-art algorithms, the computational cost of the DCT can still be prohibitive in scenarios of very low processing power or severe restrictions of energy autonomy [19, 20]. In this context, several multiplierless approximations for the DCT have been proposed [19–34]. In particular, a widely used approach is to derive approximations based on integer functions [19], such as the signum and the rounding functions. Such methodology is employed to derive the *signed DCT* (SDCT) [21] and the *rounded DCT* (RDCT) [22]. In this paper, we adopt and expand the round-off-based approximation methodology to the KLT case. We aim, therefore, at the proposition of a new class of KLT approximations. Since the transforms are defined deterministically for values of  $\rho$  in a predetermined range, our approach addresses the base exchange problem of the KLT.

This paper is structured as follows. In Section 2, we present the mathematical formulation of the KLT for first-order Markov data, the approximation theory, and the design methodology for the proposed approximations. In Section 3, the proposed transforms are presented, as well as its assessment measurements. In Subsection 3.2, the fast algorithms of the proposed transforms are displayed. Section 4 presents the experiments on image compression and Section 5 concludes the paper.

## 2 KLT and Approximate Transforms

### 2.1 KLT for First-Order Markov Signal

Let  $\mathbf{x} = [x_0 \ x_1 \ \dots \ x_{N-1}]^\top$  be an  $N$ -point random vector. The Karhunen-Loève transform is an  $N \times N$  matrix  $\mathbf{K}_N^\rho$  that maps  $\mathbf{x}$  into the  $N$ -point uncorrelated vector  $\mathbf{y} = [y_0 \ y_1 \ \dots \ y_{N-1}]^\top$  given by:

$$\mathbf{y} = \mathbf{K}_N^\rho \cdot \mathbf{x}.$$

\*Programa de Pós-Graduação em Estatística, Universidade Federal de Pernambuco, Recife, Brazil. E-mail: apr1@de.ufpe.br

†Departamento de Estatística and LACESM, Universidade Federal de Santa Maria, Santa Maria, Brazil. E-mail: bayer@ufsm.br

‡Signal Processing Group, CCEN, UFPE, Brazil. E-mail: rjds@de.ufpe.br

If  $\mathbf{x}$  is a first-order Markov signal, then it was shown in [12] that the  $(i, j)$ th entry of the KLT matrix for a given value of the correlation coefficient  $\rho \in [0, 1]$  is [9]:

$$k_{i,j} = \sqrt{\frac{2}{N + \lambda_i}} \sin \left[ \omega_i \left( i - \frac{N-1}{2} \right) + \frac{(j+1)\pi}{2} \right],$$

where  $i, j = 0, 1, \dots, N-1$ ,

$$\lambda_i = \frac{1 - \rho^2}{1 + \rho^2 - 2\rho \cos \omega_i},$$

and  $\omega_1, \omega_2, \dots, \omega_N$  are the solutions to

$$\tan N\omega = \frac{-(1 - \rho^2) \sin \omega}{(1 + \rho^2) \cos \omega - 2\rho}.$$

Since the implementation of the KLT requires floating-point arithmetic, its use has become impractical in real-time applications. In this context, low-complexity approximations for the KLT are viable solutions to circumvent this problem, since its elements generally require only trivial multiplications and bit-shifting operations.

## 2.2 Approximation Theory

Generally, an approximation is a transform  $\hat{\mathbf{T}}$  that behaves similarly to the exact transform according to some specified figure of merit. The design of approximate transforms often requires the approximations to be orthogonal [9]. Indeed, if a matrix is orthogonal, then its inverse is equal to its transpose, and its inverse is ensured to possess low complexity. However, finding orthogonal low-complexity matrices is not always an easy task. In [19], it was shown that if  $\mathbf{T}$  is a low-complexity matrix, we can obtain  $\hat{\mathbf{T}}$  through the polar decomposition [35]. Thus, we have that  $\hat{\mathbf{T}} = \mathbf{S} \cdot \mathbf{T}$ , where

$$\mathbf{S} = \begin{cases} \sqrt{(\mathbf{T} \cdot \mathbf{T}^\top)^{-1}}, & \text{if } \mathbf{T} \text{ is orthogonal,} \\ \sqrt{[\text{diag}(\mathbf{T} \cdot \mathbf{T}^\top)]^{-1}}, & \text{if } \mathbf{T} \text{ is non-orthogonal,} \end{cases} \quad (1)$$

and  $\sqrt{\cdot}$  represents the matrix square root operator [35]. Because  $\mathbf{S}$  is a diagonal matrix, the computational complexity of  $\hat{\mathbf{T}}$  is the same as that of  $\mathbf{T}$ , except for the multipliers contained in  $\mathbf{S}$ . However, the complexity of  $\mathbf{S}$  can be absorbed into other sections of a larger procedure, such as the quantization step in the context of image and video compression [20, 22, 24, 36–38]. In such cases,  $\mathbf{S}$  does not contribute to the computational cost [9, 39]. In the Appendix, we provide a brief derivation showing how the matrix  $\mathbf{S}$  can be absorbed into the quantization matrix.

## 2.3 Design Methodology

In a similar fashion as introduced in [22], the low-complexity matrix associated with the rounded KLT (RKLT) is proposed according to the following expression:

$$\mathbf{T} \triangleq \text{round}(\alpha \cdot \mathbf{K}_N^{(\rho)}), \quad (2)$$

where  $\alpha$  is an expansion factor [9],  $\mathbf{K}_N^{(\rho)}$  is the  $N$ -point KLT matrix for a first-order Markov signal with a given correlation coefficient  $0 < \rho < 1$ , and the function  $\text{round}(x) = \lfloor x + 0.5 \rfloor$ , with  $\lfloor x \rfloor = \max\{m \in \mathbb{Z} | m \leq x\}$ . When applied to a matrix, the round function operates element-wise. To ensure the low-complexity of  $\mathbf{T}$ , we restrict its entries to the set  $\{0, \pm 1\}$ . Therefore,  $\alpha$  must satisfy the inequality:  $0 \leq \text{round}(\alpha \cdot \gamma) \leq 1$ , where  $\gamma$  is the absolute value of the largest element of the matrix  $\mathbf{K}_N^{(\rho)}$ . Thus, we have  $\alpha \in [0, 3/2\gamma]$ .

## 3 Proposed Approximations

To numerically derive the proposed RKLT transforms, we adopted the procedure presented in Algorithm 1.

---

**Algorithm 1** Pseudocode for deriving low-complexity matrices.

---

**Input:**  $N, \alpha$ , step

**Output:** Set  $\mathcal{C}$  of low-complexity matrices

$\mathcal{C} = \{\}, \mathbf{T} = \mathbf{0}_{N \times N}$ ;

**for**  $\rho = \text{step} : \text{step} : (1 - \text{step})$  **do**

$\mathbf{T}' := \text{round}(\alpha \cdot \mathbf{K}_N^{(\rho)})$ ;

**if**  $\mathbf{T}' \neq \mathbf{T}$  **then**

$\mathcal{C} := \mathcal{C} \cup \{\mathbf{T}'\}$ ;

$\mathbf{T} := \mathbf{T}'$ ;

**end if**

**end for**

**return**  $\mathcal{C}$

---

The extreme values  $\rho = 0$  and  $\rho = 1$  were not considered, because they result, respectively, in a degenerate covariance matrix and in the exact DCT matrix, whose approximation theory is covered in [9]. Such methodology is capable of finding approximation for any blocklength  $N$ . In this paper, we focus on the case  $N = 8$  due to its wide significance in the image and video coding. In this case, the range of  $\alpha$  is approximately  $[0, 3.07]$ . Thus, we adopted  $\alpha = 2$ , agreeing with the methodology [40] employed to derive the RDCT [22]. Exact KLT matrices were obtained for values of  $\rho \in [0.1, 0.9]$  with steps of  $10^{-1}$ . Table 1 presents the obtained transforms and their respective diagonals  $\mathbf{S}$ , as well as the intervals of  $\rho$ . Matrix  $\mathbf{T}_4$  coincides with the transformation shown in [22].

## 3.1 Assessment Metrics

To evaluate the performance of the proposed transforms, we considered two types of figures of merit: (i) coding measures, such as the unified coding gain [41] and transform efficiency [42], which measure decorrelation and energy compaction; and (ii) proximity measures, such as the mean square error [9] and total error energy [22], which measure similarities between approximate and exact matrices in a Euclidean distance sense. We detailed each of these measures below.

### 3.1.1 Unified Coding Gain

The unified coding gain quantifies the energy compaction capability of the transform  $\hat{\mathbf{T}}$  and is given by [41]:

$$\text{Cg}(\hat{\mathbf{T}}) = 10 \cdot \log_{10} \left\{ \prod_{k=1}^N \frac{1}{\sqrt{A_k \cdot B_k}} \right\},$$

where  $A_k = \text{su} \{ (\mathbf{h}_k^\top \cdot \mathbf{h}_k) \odot \mathbf{R}_x \}$ ,  $\mathbf{h}_k$  is the  $k$ th row vector from  $\hat{\mathbf{T}}$ , the function  $\text{su}(\cdot)$  returns the sum of the elements of its matrix argument,  $\odot$  is the Hadamard matrix product operator [43],  $\mathbf{R}_x$  is the autocorrelation matrix of the considered first-order Markov signal,  $B_k = \|\mathbf{g}_k\|^2$ ,  $\mathbf{g}_k$  is the  $k$ th row vector from  $\hat{\mathbf{T}}^{-1}$ , and  $\|\cdot\|$  is the Frobenius norm [43].

Table 1: RKLTL approximations

Transform	$\rho$	Matrix	$\mathbf{S}$
$\mathbf{T}_1$	(0,0.4)	$\begin{bmatrix} 0 & 1 & 1 & 1 & 1 & -1 & -1 & 0 \\ 1 & 1 & 1 & 0 & 0 & -1 & -1 & -1 \\ 1 & 1 & 0 & -1 & -1 & 0 & 1 & 1 \\ 1 & 0 & -1 & -1 & 1 & 1 & 0 & -1 \\ 1 & 0 & -1 & 1 & 1 & -1 & 0 & 1 \\ 1 & -1 & 0 & 1 & -1 & 0 & 1 & -1 \\ 1 & -1 & 1 & 0 & 0 & 1 & -1 & 1 \\ 0 & -1 & 1 & -1 & 1 & -1 & 1 & 0 \end{bmatrix}$	$\text{diag}\left(\frac{1}{\sqrt{6}}, \frac{1}{\sqrt{6}}, \frac{1}{\sqrt{6}}, \frac{1}{\sqrt{6}}, \frac{1}{\sqrt{6}}, \frac{1}{\sqrt{6}}, \frac{1}{\sqrt{6}}, \frac{1}{\sqrt{6}}\right)$
$\mathbf{T}_2$	[0.4,0.7)	$\begin{bmatrix} 0 & 1 & 1 & 1 & 1 & 1 & 1 & 0 \\ 1 & 1 & 1 & 0 & 0 & -1 & -1 & -1 \\ 1 & 1 & 0 & -1 & -1 & 0 & 1 & 1 \\ 1 & 0 & -1 & -1 & 1 & 1 & 0 & -1 \\ 1 & -1 & -1 & 1 & 1 & -1 & 1 & 1 \\ 1 & -1 & 0 & 1 & -1 & 0 & 1 & -1 \\ 0 & -1 & 1 & 0 & 0 & 1 & -1 & 0 \\ 0 & -1 & 1 & -1 & 1 & -1 & 1 & 0 \end{bmatrix}$	$\text{diag}\left(\frac{1}{\sqrt{6}}, \frac{1}{\sqrt{6}}, \frac{1}{\sqrt{6}}, \frac{1}{\sqrt{6}}, \frac{1}{2\sqrt{2}}, \frac{1}{\sqrt{6}}, \frac{1}{2}, \frac{1}{\sqrt{6}}\right)$
$\mathbf{T}_3$	[0.7,0.8)	$\begin{bmatrix} 1 & 1 & 1 & 1 & 1 & 1 & 1 & 1 \\ 1 & 1 & 1 & 0 & 0 & -1 & -1 & -1 \\ 1 & 1 & 0 & -1 & -1 & 0 & 1 & 1 \\ 1 & 0 & -1 & -1 & 1 & 1 & 0 & -1 \\ 1 & -1 & -1 & 1 & 1 & -1 & 1 & 1 \\ 1 & -1 & 0 & 1 & -1 & 0 & 1 & -1 \\ 0 & -1 & 1 & 0 & 0 & 1 & -1 & 0 \\ 0 & -1 & 1 & -1 & 1 & -1 & 1 & 0 \end{bmatrix}$	$\text{diag}\left(\frac{1}{2\sqrt{2}}, \frac{1}{\sqrt{6}}, \frac{1}{\sqrt{6}}, \frac{1}{\sqrt{6}}, \frac{1}{2\sqrt{2}}, \frac{1}{\sqrt{6}}, \frac{1}{2}, \frac{1}{\sqrt{6}}\right)$
$\mathbf{T}_4$ [22]	[0.8,1)	$\begin{bmatrix} 1 & 1 & 1 & 1 & 1 & 1 & 1 & 1 \\ 1 & 1 & 1 & 0 & 0 & -1 & -1 & -1 \\ 1 & 0 & 0 & -1 & -1 & 0 & 0 & 1 \\ 1 & 0 & -1 & -1 & 1 & 1 & 0 & -1 \\ 1 & -1 & -1 & 1 & 1 & -1 & 1 & 1 \\ 1 & -1 & 0 & 1 & -1 & 0 & 1 & -1 \\ 0 & -1 & 1 & 0 & 0 & 1 & -1 & 0 \\ 0 & -1 & 1 & -1 & 1 & -1 & 1 & 0 \end{bmatrix}$	$\text{diag}\left(\frac{1}{2\sqrt{2}}, \frac{1}{\sqrt{6}}, \frac{1}{2}, \frac{1}{\sqrt{6}}, \frac{1}{2\sqrt{2}}, \frac{1}{\sqrt{6}}, \frac{1}{2}, \frac{1}{\sqrt{6}}\right)$

### 3.1.2 Transform Efficiency

The transform efficiency is another coding related figure of merit, and is given by [42]:

$$\eta(\hat{\mathbf{T}}) = 100 \cdot \frac{\sum_{i=1}^N |r_{i,i}|}{\sum_{i=1}^N \sum_{j=1}^N |r_{i,j}|},$$

where  $r_{i,j}$  is the  $(i,j)$ th element from  $\hat{\mathbf{T}} \cdot \mathbf{R}_{\mathbf{x}} \cdot \hat{\mathbf{T}}^\top$ .

### 3.1.3 Mean Square Error

The mean square error (MSE) relative to the exact KLT is given by [9]:

$$\text{MSE}(\hat{\mathbf{T}}) = \frac{1}{N} \cdot \text{tr} \left\{ (\mathbf{K}_N^{(\rho)} - \hat{\mathbf{T}} \cdot \mathbf{R}_{\mathbf{x}} \cdot (\mathbf{K}_N^{(\rho)} - \hat{\mathbf{T}})^\top) \right\},$$

where  $\text{tr}(\cdot)$  is the trace function [44].

### 3.1.4 Total Error Energy

Another error measure is the total error energy, which is given by [22]:

$$\epsilon(\hat{\mathbf{T}}) = \pi \cdot \|\mathbf{K}_N^{(\rho)} - \hat{\mathbf{T}}\|^2.$$

Strictly there is no competing method in the literature that could allow us to make a fair comparison. Thus, we compared the proposed approximation only with the exact KLT for  $\rho = 0.3, 0.4, 0.7$ , and  $0.8$ . We considered the exact same values of  $\rho$  for computing the unified coding gain and the transform efficiency, which depends on the autocorrelation matrix  $\mathbf{R}_{\mathbf{x}}$  of the considered first-order Markov input signal. Thus, we assessed  $\hat{\mathbf{T}}_1$  compared to the  $\mathbf{K}^{(0.3)}$  for the value of  $\rho = 0.3$ ,  $\hat{\mathbf{T}}_2$  compared to the  $\mathbf{K}^{(0.4)}$  for the value of  $\rho = 0.4$ ,  $\hat{\mathbf{T}}_3$  compared to the  $\mathbf{K}^{(0.7)}$  for the value of  $\rho = 0.7$ , and  $\hat{\mathbf{T}}_4$  compared to the  $\mathbf{K}^{(0.8)}$  for the value of  $\rho = 0.8$ .

To the best of our knowledge, the literature lacks efficient KLT-based methods for lowly correlated data. We aim at contributing to filling this gap.

Table 2 presents the coding and similarity measurements. As reference values, the total error energy and mean square error for the RDCT [22] compared to the DCT (for  $\rho = 0.95$ ) are, respectively, 1.7945 and 0.0098. Note that for the proximity measures (mean square error and total error energy), the proposed transforms perform well, even better than the performance of the RDCT compared to the DCT considering the total error energy. In this case, the smaller the measurement is, the more similar the approximate transform is to the exact one. Considering the coding measures (unified coding gain and transform efficiency), the proposed transforms assert their good performances when compared with the measurements from the exact KLT for each value of  $\rho$ . The exact KLT coding measurements have been used as a benchmark to evaluate the performance of other transforms since it is the unitary optimal transform in terms of energy compaction and decorrelation [9, 10]. It is notable that the performance of the proposed approximations are similar to the exact KLT and have a greatly reduced computational cost, as detailed in the following.

## 3.2 Fast Algorithm and Computational Complexity

Fast algorithms for the approximate transforms can be derived based on the sparse factorization of the transform matrices and butterfly matrix structures [39]. The factorizations of the proposed transform are given by:

$$\mathbf{T}_i = \mathbf{P}_i \cdot \mathbf{A}_{2,i} \cdot \mathbf{A}_1 \quad \text{for } i = 1, 2, 3, 4,$$

where

$$\mathbf{A}_1 = \begin{bmatrix} \mathbf{I}_4 & \bar{\mathbf{I}}_4 \\ \bar{\mathbf{I}}_4 & -\mathbf{I}_4 \end{bmatrix}, \quad \mathbf{A}_{2,i} = \begin{bmatrix} \mathbf{B}_{2,i} & \\ & \mathbf{B}_2 \end{bmatrix},$$

$$\mathbf{B}_2 = \begin{bmatrix} -1 & -1 & 0 & 1 \\ -1 & 1 & -1 & 0 \\ 1 & 0 & -1 & 1 \\ 0 & 1 & 1 & 1 \end{bmatrix},$$

Table 2: Coding and similarity measures

	$\rho$	$Cg(\hat{\mathbf{T}})$	$\eta(\hat{\mathbf{T}})$	$\epsilon(\mathbf{K}^{(\rho)}, \hat{\mathbf{T}})$	$MSE(\mathbf{K}^{(\rho)}, \hat{\mathbf{T}})$
$\mathbf{K}^{(0.3)}$	0.3	0.3584	100	0	0
$\hat{\mathbf{T}}_1$	(0,0.4)	0.2829	80.7088	1.6751	0.0659
$\mathbf{K}^{(0.4)}$	0.4	0.6626	100	0	0
$\hat{\mathbf{T}}_2$	[0.4,0.7)	0.5616	70.2996	1.7011	0.0660
$\mathbf{K}^{(0.7)}$	0.7	2.5588	100	0	0
$\hat{\mathbf{T}}_3$	[0.7,0.8)	2.1398	65.8777	1.4716	0.0523
$\mathbf{K}^{(0.8)}$	0.8	3.8824	100	0	0
$\hat{\mathbf{T}}_4$ [22]	[0.8,1)	3.4058	74.4747	1.7715	0.0362

and  $\mathbf{I}_4$  and  $\bar{\mathbf{I}}_4$  are, respectively, the identity and counter-identity matrices of order 4. Matrices  $\mathbf{B}_{2,i}$  are given by:

$$\mathbf{B}_{2,1} = \begin{bmatrix} 1 & 1 & 0 & -1 \\ 1 & -1 & 1 & 0 \\ 1 & 0 & -1 & 1 \\ 0 & 1 & 1 & 1 \end{bmatrix}, \quad \mathbf{B}_{2,2} = \begin{bmatrix} 1 & 1 & 0 & -1 \\ 1 & -1 & -1 & 1 \\ 0 & -1 & 1 & 0 \\ 0 & 1 & 1 & 1 \end{bmatrix},$$

$$\mathbf{B}_{2,3} = \begin{bmatrix} 1 & 1 & 1 & 0 \\ 1 & -1 & -1 & 0 \\ 0 & -1 & 1 & 0 \\ 0 & 1 & 0 & 1 \end{bmatrix}, \quad \begin{bmatrix} 1 & 0 & 0 & 1 \\ 0 & 1 & 0 & 0 \\ 0 & 0 & 1 & 0 \\ 1 & 0 & 0 & -1 \end{bmatrix},$$

$$\mathbf{B}_{2,4} = \begin{bmatrix} 1 & 1 & 0 & 0 \\ 1 & -1 & 0 & 0 \\ 0 & 0 & -1 & 0 \\ 0 & 0 & 0 & 1 \end{bmatrix}, \quad \begin{bmatrix} 1 & 0 & 0 & 1 \\ 0 & 1 & 1 & 0 \\ 0 & 1 & -1 & 0 \\ 1 & 0 & 0 & -1 \end{bmatrix}.$$

The permutation matrices  $\mathbf{P}_i$  are:

$$\mathbf{P}_1 = \begin{bmatrix} 0 & 0 & 0 & 1 & 0 & 0 & 0 & 0 \\ 0 & 0 & 0 & 0 & 0 & 0 & 0 & 1 \\ 1 & 0 & 0 & 0 & 0 & 0 & 0 & 0 \\ 0 & 0 & 0 & 0 & 1 & 0 & 0 & 0 \\ 0 & 0 & 1 & 0 & 0 & 0 & 0 & 0 \\ 0 & 0 & 0 & 0 & 0 & 0 & 1 & 0 \\ 0 & 1 & 0 & 0 & 0 & 0 & 0 & 0 \\ 0 & 0 & 0 & 0 & 0 & 0 & 1 & 0 \end{bmatrix},$$

$$\mathbf{P}_2 = \begin{bmatrix} 0 & 0 & 0 & 1 & 0 & 0 & 0 & 0 \\ 0 & 0 & 0 & 0 & 0 & 0 & 0 & 1 \\ 1 & 0 & 0 & 0 & 0 & 0 & 0 & 0 \\ 0 & 0 & 0 & 0 & 1 & 0 & 0 & 0 \\ 0 & 1 & 0 & 0 & 0 & 0 & 0 & 0 \\ 0 & 0 & 0 & 0 & 0 & 0 & 1 & 0 \\ 0 & 0 & 1 & 0 & 0 & 0 & 0 & 0 \\ 0 & 0 & 0 & 0 & 0 & 1 & 0 & 0 \end{bmatrix},$$

and

$$\mathbf{P}_3 = \mathbf{P}_4 = \begin{bmatrix} 1 & 0 & 0 & 0 & 0 & 0 & 0 & 0 \\ 0 & 0 & 0 & 0 & 0 & 0 & 0 & 1 \\ 0 & 0 & 0 & 1 & 0 & 0 & 0 & 0 \\ 0 & 0 & 0 & 0 & 1 & 0 & 0 & 0 \\ 0 & 1 & 0 & 0 & 0 & 0 & 0 & 0 \\ 0 & 0 & 0 & 0 & 0 & 0 & 1 & 0 \\ 0 & 0 & 1 & 0 & 0 & 0 & 0 & 0 \\ 0 & 0 & 0 & 0 & 0 & 1 & 0 & 0 \end{bmatrix}.$$

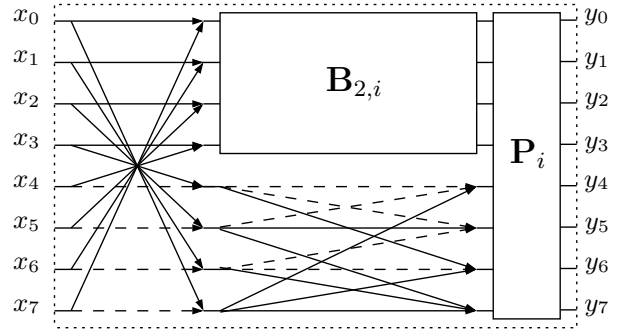


Figure 1: SFG of the proposed transforms. Block  $\mathbf{B}_{2,i}$  is different for each transform and it is presented in Fig. 2.

Fig. 1 and 2 show the signal flow graphs (SFG) of the fast algorithms. The dashed arrows represent multiplication by  $-1$ .

The direct implementation of the exact KLT requires 56 additions and 64 multiplications. The proposed transforms are designed to be multiplierless but still require 56 additions in its direct implementation. Considering the fast algorithms proposed for the transforms, we have a reduction in the addition operations relative to the direct implementation. Matrices  $\mathbf{T}_1$ ,  $\mathbf{T}_2$ , and  $\mathbf{T}_3$  require only 24 additions, causing a reduction of 57.17% in the number of addition operations, and matrix  $\mathbf{T}_4$  requires 22 additions, with a reduction of 60.71%.

## 4 Image Compression

In this section, the performance of the proposed transforms is assessed in the context of image compression [45] as suggested in [19–22, 26, 27, 46].

### 4.1 JPEG-like Compression

The following compression scheme [6] was applied to standardized images obtained from the public image bank available in [47]. Input images were divided into disjoint sub-blocks of size  $8 \times 8$ . The 2D direct and inverse transformations induced by  $\mathbf{K}_N^\rho$  are computed, respectively, by [48]:

$$\mathbf{B} = \mathbf{K}_N^\rho \cdot \mathbf{A} \cdot (\mathbf{K}_N^\rho)^{-1},$$

$$\mathbf{A} = (\mathbf{K}_N^\rho)^{-1} \cdot \mathbf{B} \cdot \mathbf{K}_N^\rho,$$

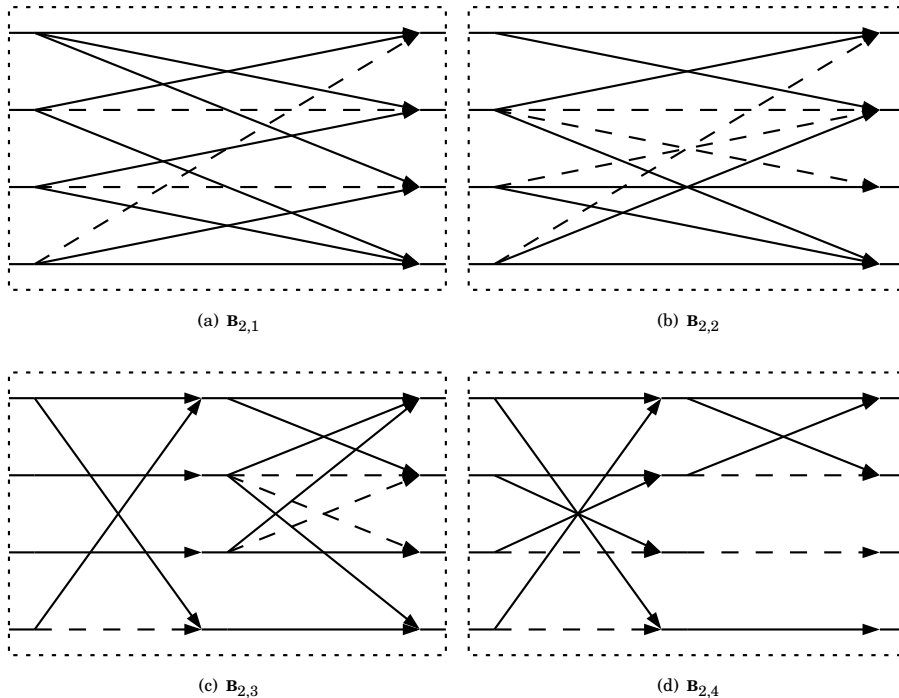


Figure 2: Block  $\mathbf{B}_{2,i}$  of each proposed transform.

where  $\mathbf{A}$  and  $\mathbf{B}$  are square matrices of size  $N$ . Each sub-block was submitted to the 2D transform computation and the resulting transform-domain coefficients were re-ordered using the standard zig-zag sequence [6]. Only the initial  $r$  coefficients in each sub-block were retained and the remaining coefficients were zeroed. The 2D inverse transform was applied and the reconstructed sub-blocks were adequately rearranged. Original and compressed images were then evaluated considering traditional quality assessment measures. The considered figures of merit for image quality evaluation were: (i) the mean structural similarity index (MSSIM) [49]; (ii) the mean square error (MSE) [9]; (iii) and the peak signal-to-noise ratio (PSNR) [50]. Even though the PSNR and MSE are very popular figures of merit, it was shown in [51] that it might offer limited results as image quality assessment tools for its poorly correlates with human perception. On the other hand, the MSSIM is capable of closely capturing the image quality as understood by the human visual system model [49].

The image compression experiments were divided into two analyses: (i) a qualitative one, based on compressed *Lena*, *Baboon*, and *Moon* images with approximately 77% of compression rate; (ii) and a quantitative analysis, based on the average measures of 45 standardized 8-bit compressed images [47] for a wide range of retained coefficients ( $r$ ). The results are presented below.

## 4.2 Results

For the qualitative analysis, we considered three known public images available on [47]. The original grayscale images are presented in Fig. 3.

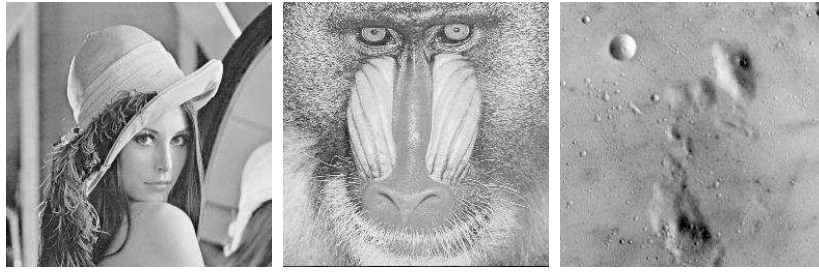
Fig. 4, 5, and 6 illustrate qualitatively the reconstruction of the *Lena*, *Baboon*, and *Moon* images, after the application of the compression scheme for  $r = 15$  (compression rate of approximately 77%) using the proposed RKLT, the exact KLT for  $\rho = 0.3, 0.4, 0.7, 0.8$ , and the exact DCT. The assessment metrics from each compressed image are presented in Table 3. We highlighted the results from

the proposed transforms which performed better than the exact KLT for the value of  $\rho$  associated with the interval of which the approximate transform was derived. Approximations  $\hat{\mathbf{T}}_2$  and  $\hat{\mathbf{T}}_3$  outperformed the exact KLT,  $\mathbf{K}^{(0.4)}$  and  $\mathbf{K}^{(0.7)}$  respectively, according to the values of MSE, PSNR, and MSSIM. The approximations may outperform the exact KLT because we measure the overall performance of the entire image compression system, which includes particular nonlinearities that are better suited for the approximate computation.

For the quantitative analysis, we considered the average image quality measurements of 45 compressed standardized images [47] considering different levels of compression ( $r \in (0, 45)$ ). Fig. 7 presents the average image quality measurements from the compressed images considering the approximate transforms and the exact KLT for values of  $\rho = 0.3, 0.4, 0.7$ , and  $0.8$ . The approximate transforms perform similarly to the exact KLT, mainly when we retain more than  $r = 15$  retained coefficients, except for  $\hat{\mathbf{T}}_1$ . Approximation  $\hat{\mathbf{T}}_4$  outperformed the exact KLT ( $\rho = 0.8$ ) for  $r \in [1, 11]$  considering PSNR values and for  $r \in [1, 14]$  considering the MSSIM values. Considering the performance in JPEG-like compression the proposed approximations exhibited relevant results, showing a good balance between performance and computational cost.

## 5 Conclusions

In this paper, we introduced a methodology based on the rounding-off function to design low-complexity approximations for the Karhunen-Loève transform (KLT). Due to its relevance in practical image coding systems, the special case  $N = 8$  was comprehensively examined. According to qualitative and quantitative computation experiments, the proposed transforms were shown to be good approximations for KLT as measured by the adopted quality measures: MSE, PSNR, and MSSIM. The low-complexity matrices are natural candidates for the design of efficient hardware imple-



(a) *Lena*

(b) *Baboon*

(c) *Moon*

Figure 3: Original images.



(a)  $\hat{\mathbf{T}}_1$

(b)  $\hat{\mathbf{T}}_2$

(c)  $\hat{\mathbf{T}}_3$

(d)  $\hat{\mathbf{T}}_4$  [22]



(e)  $\mathbf{K}^{(0.3)}$

(f)  $\mathbf{K}^{(0.4)}$

(g)  $\mathbf{K}^{(0.7)}$

(h)  $\mathbf{K}^{(0.8)}$



(i) DCT

Figure 4: Compressed *Lena* images.

mentation capable of operating at low power consumption and high performance.

*nambuco (FACEPE)*, Brazil.

## Acknowledgements

We gratefully acknowledge partial financial support from *Coordenação de Aperfeiçoamento de Pessoal de Nível Superior (CAPES)*, *Conselho Nacional de Desenvolvimento Científico e Tecnológico (CNPq)* and *Fundação de Amparo à Ciência e Tecnologia de Per-*

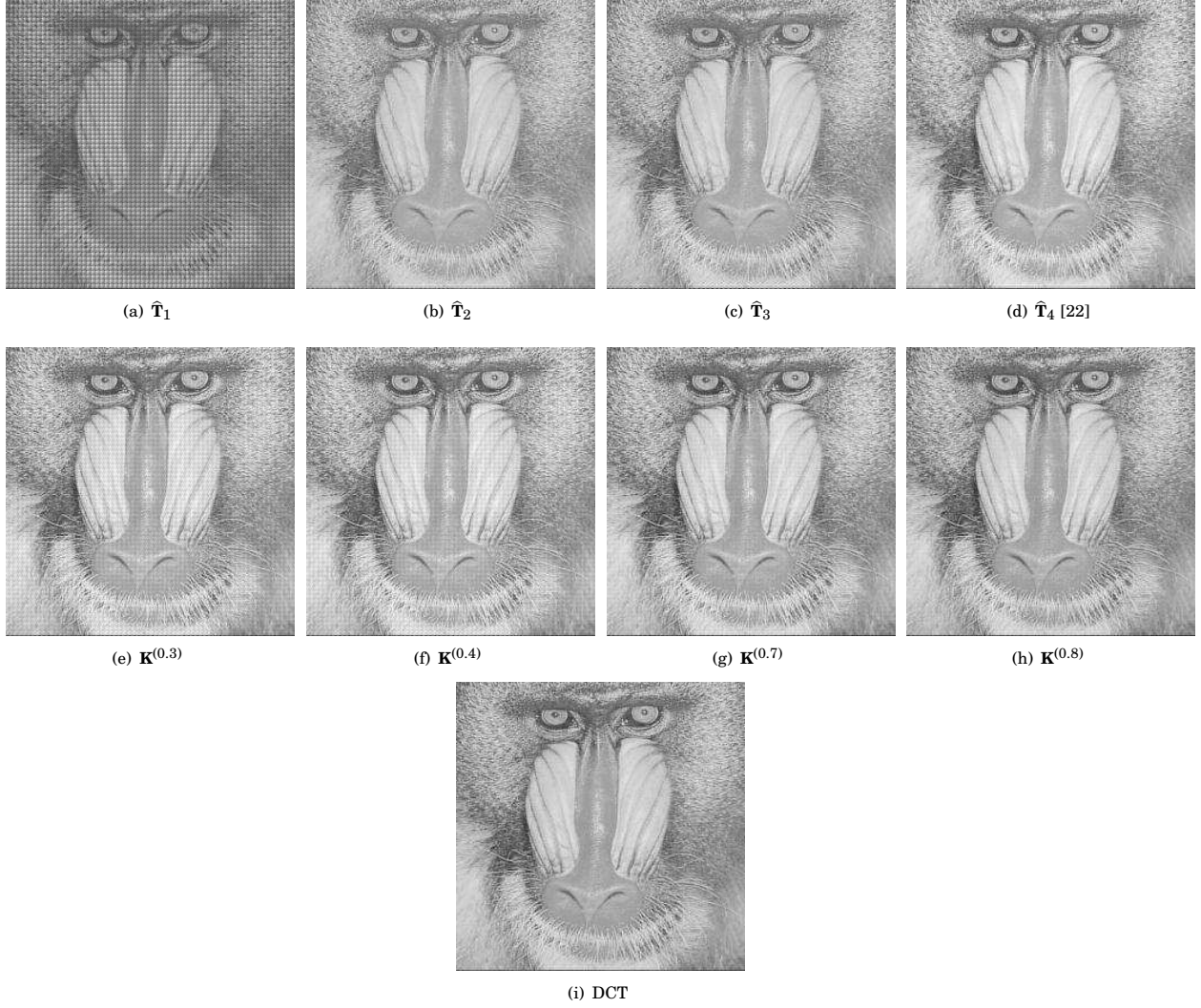


Figure 5: Compressed *Baboon* images.

## A 2D transformation and quantization step

Let  $\mathbf{A}$  be a  $8 \times 8$  sub-block from an image. The 2D transformation from  $\mathbf{A}$  induced by an approximation  $\hat{\mathbf{T}}$  is given by:

$$\begin{aligned}
 \mathbf{B} &= \begin{cases} \hat{\mathbf{T}} \cdot \mathbf{A} \cdot \hat{\mathbf{T}}^\top, & \text{if } \mathbf{T} \text{ is orthogonal,} \\ \hat{\mathbf{T}} \cdot \mathbf{A} \cdot \hat{\mathbf{T}}^{-1}, & \text{if } \mathbf{T} \text{ is non-orthogonal,} \end{cases} \\
 &= \begin{cases} (\mathbf{u} \cdot \mathbf{u}^\top) \odot (\mathbf{T} \cdot \mathbf{A} \cdot \mathbf{T}^\top), & \text{if } \mathbf{T} \text{ is orthogonal,} \\ (\mathbf{u} \cdot \mathbf{v}^\top) \odot (\mathbf{T} \cdot \mathbf{A} \cdot \mathbf{T}^{-1}), & \text{if } \mathbf{T} \text{ is non-orthogonal,} \end{cases} \\
 &= \mathbf{R} \odot \hat{\mathbf{B}}, \tag{3}
 \end{aligned}$$

where  $\mathbf{u} = \text{diag}(\mathbf{S})$  and  $\mathbf{v}$  is given by the inverse elements from  $\mathbf{u}$ . In the context of JPEG-like compression [16], the quantized coefficient matrix  $\hat{\mathbf{B}}$  is given by:

$$\hat{\mathbf{B}} = \text{round}(\mathbf{B} \div \mathbf{Q}), \tag{4}$$

where  $\mathbf{Q}$  is a quantization matrix and  $\div$  denotes the element-wise matrix division.

By applying Equation (3) in (4), we obtain

$$\bar{\mathbf{B}} = \text{round}(\mathbf{R} \odot \hat{\mathbf{B}} \div \mathbf{Q}) = \text{round}(\hat{\mathbf{B}} \div \hat{\mathbf{Q}}),$$

where  $\hat{\mathbf{Q}} = \mathbf{Q} \div \mathbf{R}$ . Note that  $\mathbf{R}$  can be absorbed in the quantization step, thus, the complexity of matrix  $\mathbf{S}$  can be dismissed in the image compression applications [5, 6, 45].

## References

- [1] D. Goldston, "Big data: Data wrangling," *Nature News*, vol. 455, no. 7209, p. 15–15, 2008.
- [2] F. Betzel, K. Khatamifard, H. Suresh, D. J. Lilja, J. Sartori, and U. Karpuzcu, "Approximate communication: Techniques for reducing communication bottlenecks in large-scale parallel systems," *ACM Computing Surveys (CSUR)*, vol. 51, no. 1, pp. 1–32, 2018.
- [3] W. B. Pennebaker and J. L. Mitchell, *JPEG: Still image data compression standard*. Springer Science & Business Media, 1992.
- [4] I. T. Jolliffe, *Principal Component Analysis*. Springer-Verlag New York, 1986.
- [5] K. Sayood, *Introduction to data compression*. Morgan Kaufmann, 2017.
- [6] D. Salomon, *Data compression: the complete reference*. Springer Science & Business Media, 2004.
- [7] K. Karhunen, "Under lineare methoden in der wahr scheinlichkeit-rechnung," *Annales Academiae Scientiarum Fennicae Series A1: Mathematica Physica*, vol. 47, 1947.

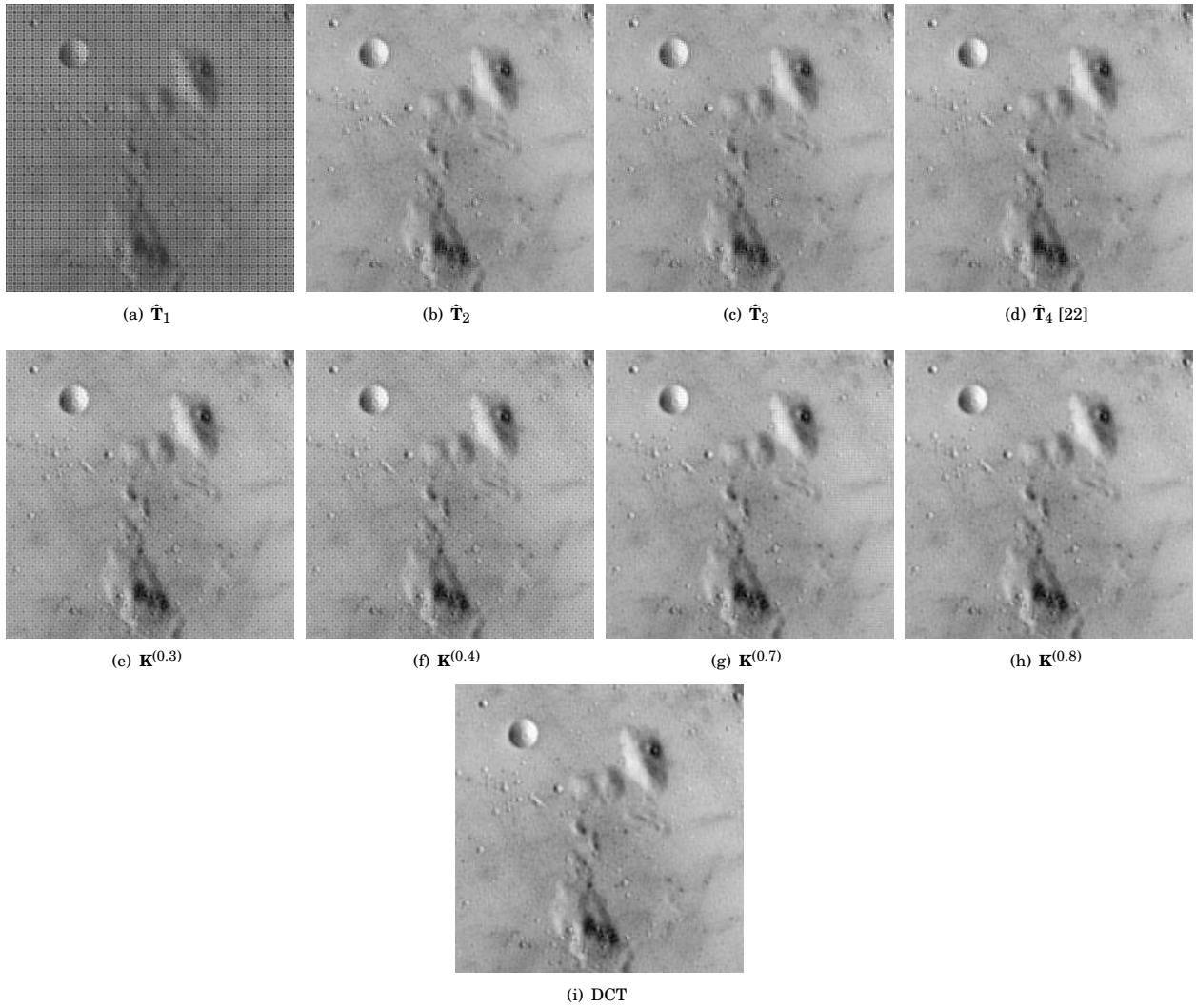


Figure 6: Compressed *Moon* images.

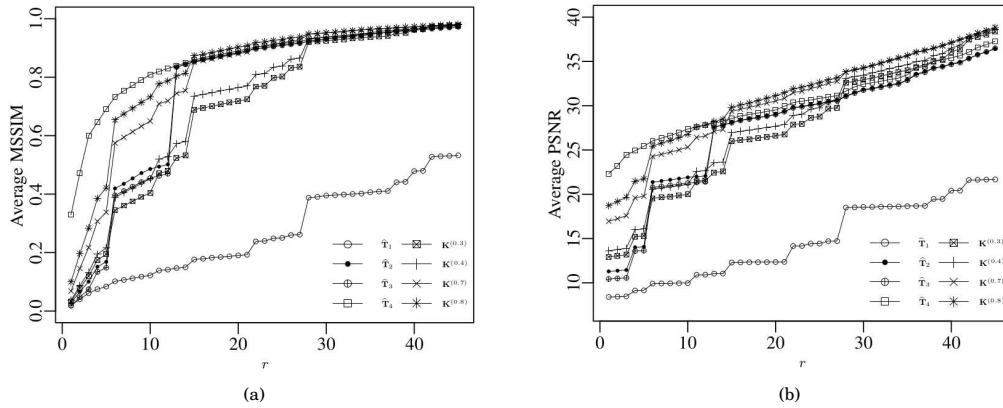


Figure 7: Image quality measurements for different levels of compression.

[8] M. Loève, “Fonctions aléatoires de second ordre,” *Processus Stochastique et Mouvement Brownien*, p. 366–420, 1948.  
 [9] V. Britanak, P. C. Yip, and K. R. Rao, *Discrete cosine and sine transforms: general properties, fast algorithms and integer approximations*. Academic Press, 2010.  
 [10] H. Ochoa-Dominguez and K. R. Rao, *Discrete Cosine Transform*. CRC

Press, 2019.

[11] W. Ray and R. Driver, “Further decomposition of the Karhunen-Loève series representation of a stationary random process,” *IEEE Transactions on Information Theory*, vol. 16, no. 6, p. 663–668, 1970.  
 [12] A. K. Jain, “A fast Karhunen-Loève transform for a class of random



Table 3: Quality image assessment measurements for *Lena*, *Baboon*, and *Moon* compressed images

Image	Lena			Baboon			Moon		
	MSE	PSNR	MSSIM	MSE	PSNR	MSSIM	MSE	PSNR	MSSIM
$\hat{\mathbf{T}}_1$	3198.18	13.082	0.154	3505.908	12.683	0.220	3114.159	13.197	0.096
$\mathbf{K}^{(0.3)}$	95.674	28.323	0.660	322.113	23.051	0.685	112.060	27.636	0.598
$\hat{\mathbf{T}}_2$	48.729	31.253	<b>0.913</b>	313.852	23.164	<b>0.761</b>	<b>57.287</b>	<b>30.550</b>	<b>0.781</b>
$\mathbf{K}^{(0.4)}$	70.215	29.666	0.720	296.260	23.414	0.716	87.816	28.695	0.653
$\hat{\mathbf{T}}_3$	49.071	31.222	<b>0.913</b>	313.788	23.164	0.761	57.276	30.551	<b>0.781</b>
$\mathbf{K}^{(0.7)}$	30.464	33.293	0.884	257.115	24.030	0.783	50.058	31.136	0.776
$\hat{\mathbf{T}}_4$ [22]	44.593	31.638	0.917	286.597	23.558	0.766	52.478	30.931	0.789
$\mathbf{K}^{(0.8)}$	25.907	33.997	0.916	253.406	24.093	0.793	45.705	31.531	0.796
DCT	23.867	34.353	0.938	254.233	24.078	0.796	43.543	31.742	0.807

- processes,” *IEEE Transactions on Communications*, vol. 24, no. 9, p. 1023–1029, 1976.
- [13] I. S. Reed and L.-S. Lan, “A fast approximate Karhunen-Loève transform (AKLT) for data compression,” *Journal of Visual Communication and Image Representation*, vol. 5, no. 4, p. 304–316, 1994.
- [14] K. Fan, R. Wang, W. Lin, L.-Y. Duan, and W. Gao, “Signal-independent separable KLT by offline training for video coding,” *IEEE Access*, vol. 7, p. 33087–33093, 2019.
- [15] N. Ahmed, T. Natarajan, and K. R. Rao, “Discrete cosine transform,” *IEEE Transactions on Computers*, vol. C-23, no. 1, p. 90–93, 1974.
- [16] G. K. Wallace, “The JPEG still picture compression standard,” *IEEE Transactions on Consumer Electronics*, vol. 38, no. 1, p. xviii–xxxiv, 1992.
- [17] A. Puri, “Video coding using the H.264/MPEG-4 AVC compression standard,” *Signal Processing: Image Communication*, vol. 19, 2004.
- [18] M. T. Pourazad, C. Doutre, M. Azimi, and P. Nasiopoulos, “HEVC: The new gold standard for video compression: How does HEVC compare with H.264/AVC?,” *IEEE Consumer Electronics Magazine*, vol. 1, no. 3, p. 36–46, 2012.
- [19] R. J. Cintra, F. M. Bayer, and C. Tablada, “Low-complexity 8-point DCT approximations based on integer functions,” *Signal Processing*, vol. 99, p. 201–214, 2014.
- [20] S. Bouguezel, M. O. Ahmad, and M. Swamy, “Low-complexity 8×8 transform for image compression,” *Electronics Letters*, vol. 44, no. 21, p. 1249–1250, 2008.
- [21] T. I. Haweel, “A new square wave transform based on the DCT,” *Signal Processing*, vol. 81, no. 11, p. 2309–2319, 2001.
- [22] R. J. Cintra and F. M. Bayer, “A DCT approximation for image compression,” *IEEE Signal Processing Letters*, vol. 18, no. 10, p. 579–582, 2011.
- [23] U. S. Potluri, A. Madanayake, R. J. Cintra, F. M. Bayer, S. Kulasekera, and A. Edirisuriya, “Improved 8-point approximate DCT for image and video compression requiring only 14 additions,” *IEEE Transactions on Circuits and Systems I: Regular Papers*, vol. 61, no. 6, p. 1727–1740, 2014.
- [24] F. M. Bayer and R. J. Cintra, “DCT-like transform for image compression requires 14 additions only,” *Electronics Letters*, vol. 48, no. 15, p. 919–921, 2012.
- [25] M. Jridi, A. Alfalou, and P. K. Meher, “A generalized algorithm and reconfigurable architecture for efficient and scalable orthogonal approximation of DCT,” *IEEE Transactions on Circuits and Systems I: Regular Papers*, vol. 62, no. 2, p. 449–457, 2015.
- [26] T. L. da Silveira, R. S. Oliveira, F. M. Bayer, R. J. Cintra, and A. Madanayake, “Multiplierless 16-point DCT approximation for low-complexity image and video coding,” *Signal, Image and Video Processing*, vol. 11, no. 2, p. 227–233, 2017.
- [27] R. S. Oliveira, R. J. Cintra, F. M. Bayer, T. L. da Silveira, A. Madanayake, and A. Leite, “Low-complexity 8-point DCT approximation based on angle similarity for image and video coding,” *Multidimensional Systems and Signal Processing*, vol. 30, no. 3, p. 1363–1394, 2019.
- [28] D. R. Canterle, T. L. da Silveira, F. M. Bayer, and R. J. Cintra, “A multiparametric class of low-complexity transforms for image and video coding,” *Signal Processing*, vol. 176, p. 107685, 2020.
- [29] A. Singhadia, P. Bante, and I. Chakrabarti, “A novel algorithmic approach for efficient realization of 2-D-DCT architecture for HEVC,” *IEEE Transactions on Consumer Electronics*, vol. 65, no. 3, pp. 264–273, 2019.
- [30] D. Puchala, “Approximate calculation of 8-point DCT for various scenarios of practical applications,” *EURASIP Journal on Image and Video Processing*, vol. 2021, no. 1, pp. 1–34, 2021.
- [31] N. Zidani, N. Kouadria, N. Doghmane, and S. Harize, “Low complexity pruned DCT approximation for image compression in wireless multimedia sensor networks,” in *2019 5th International Conference on Frontiers of Signal Processing (ICFSP)*, pp. 26–30, IEEE, 2019.
- [32] J. Chen, S. Liu, G. Deng, and S. Rahardja, “Hardware efficient integer discrete cosine transform for efficient image/video compression,” *IEEE Access*, vol. 7, pp. 152635–152645, 2019.
- [33] J. Huang, T. N. Kumar, H. A. Almurib, and F. Lombardi, “A deterministic low-complexity approximate (multiplier-less) technique for DCT computation,” *IEEE Transactions on Circuits and Systems I: Regular Papers*, vol. 66, no. 8, pp. 3001–3014, 2019.
- [34] D. F. Coelho, R. J. Cintra, A. Madanayake, and S. M. Perera, “Low-complexity scaling methods for DCT-II approximations,” *IEEE Transactions on Signal Processing*, pp. 1–1, 2021.
- [35] N. J. Higham, *Functions of matrices: theory and computation*, vol. 104. Philadelphia, PA: SIAM, 2008.
- [36] S. Bouguezel, M. O. Ahmad, and M. N. S. Swamy, “A low-complexity parametric transform for image compression,” in *IEEE International Symposium of Circuits and Systems (ISCAS)*, p. 2145–2148, 2011.
- [37] K. Lengwehasatit and A. Ortega, “Scalable variable complexity approximate forward DCT,” *IEEE Transactions on Circuits and Systems for Video Technology*, vol. 14, no. 11, p. 1236–1248, 2004.
- [38] F. M. Bayer, R. J. Cintra, A. Edirisuriya, and A. Madanayake, “A digital hardware fast algorithm and FPGA-based prototype for a novel 16-point approximate DCT for image compression applications,” *Measurement Science and Technology*, vol. 23, no. 11, p. 114010, 2012.
- [39] R. E. Blahut, *Fast algorithms for signal processing*. Cambridge University Press, 2010.
- [40] R. J. Cintra, “An integer approximation method for discrete sinusoidal transforms,” *Circuits, Systems, and Signal Processing*, vol. 30, no. 6, p. 1481, 2011.

- [41] J. Katto, K. Komatsu, and Y. Yasuda, "Short-tap and linear-phase PR filter banks for subband coding of images," in *Visual Communications and Image Processing'92*, vol. 1818, p. 735–747, International Society for Optics and Photonics, 1992.
- [42] J. Takala and J. Nikara, "Unified pipeline architecture for discrete sine and cosine transforms of type IV," in *Proceedings of the 3rd International Conference on Information Communication and Signal Processing*, 2001.
- [43] G. A. Seber, *A matrix handbook for statisticians*, vol. 15. John Wiley & Sons, 2008.
- [44] D. A. Harville, "Trace of a (square) matrix," in *Matrix Algebra From a Statistician's Perspective*, p. 49–53, Springer, 1997.
- [45] R. C. Gonzalez, R. E. Woods, et al., *Digital image processing*. Upper Saddle River, NJ: Prentice hall, 2002.
- [46] M. Jridi, A. Alfalou, and P. K. Meher, "A generalized algorithm and reconfigurable architecture for efficient and scalable orthogonal approximation of DCT," *IEEE Transactions on Circuits and Systems I: Regular Papers*, vol. 62, no. 2, p. 449–457, 2015.
- [47] U. SIPI, "The USC-SIPI image database," 1977.
- [48] T. Suzuki and M. Ikehara, "Integer DCT based on direct-lifting of DCT-IDCT for lossless-to-lossy image coding," *IEEE Transactions on Image Processing*, vol. 19, no. 11, p. 2958–2965, 2010.
- [49] Z. Wang, A. C. Bovik, H. R. Sheikh, and E. P. Simoncelli, "Image quality assessment: from error visibility to structural similarity," *IEEE Transactions on Image Processing*, vol. 13, no. 4, p. 600–612, 2004.
- [50] Q. Huynh-Thu and M. Ghanbari, "Scope of validity of PSNR in image/video quality assessment," *Electronics Letters*, vol. 44, no. 13, p. 800–801, 2008.
- [51] Z. Wang and A. C. Bovik, "Mean squared error: Love it or leave it? a new look at signal fidelity measures," *IEEE Signal Processing Magazine*, vol. 26, no. 1, pp. 98–117, 2009.